Advances in Social Science, Education and Humanities Research, volume 576
Proceedings of the 2nd International Conference on Science, Technology, and Modern Society (ICSTMS 2020)

Optical Properties of Fe_3O_4/Chitosan and Its Applications for Signal Amplifier in Surface Plasmon Resonance Sensor

I. P. T. Indrayana*
[1] Physics Study Program, [2] Department of Physics
[1] Universitas Halmahera, [2] Universitas Udayana
[1] Maluku Utara, Indonesia, [2] Bali, Indonesia
*tedyindrayana@gmail.com

M. T. Tuny
Forestry Study Program
Universitas Halmahera
Maluku Utara, Indonesia

R. A. Putra
Physics Study Program, Faculty of Engineering
Universitas Samudra
Indonesia

N. I. Istiqomah, Juharni, E. Suharyadi
Department of Physics
Universitas Gadjah Mada
Yogyakarta, Indonesia

***Abstract*—The Fe3O4/chitosan nanocomposite is one of the attractive functional materials. It can be applied as active material in a sensor system for an instant Surface Plasmon Resonance (SPR) based sensor. This research aimed at investigating the optical properties of Fe_3O_4/chitosan and its effect on the SPR angle. The synthesis of nanoparticles used the coprecipitation method. Encapsulation was carried out at a temperature of 50ºC for about 60 minutes. The samples were characterized for their structural properties and phase composition by using X-ray diffraction (XRD) techniques. Their optical properties were characterized by using the Specular Reflectance UV-Vis Spectroscopy technique. The optical properties, such as absorbance (*A*), absorption coefficient (α), refractive index (*n*), extinction coefficient (*k*), optical gap energy (Eg), and Urbach energy (Eu) are investigated. The measurement of the SPR angle toward the ATR curve was carried out in a range of 30º – 60º by using the Kretschmann configuration. The results show that encapsulation affects the optical properties of the nanoparticles. The SPR angle of prism/Au/Fe_3O_4/Air and prism/Au/Fe_3O_4-Chitosan/Air system is about 50.04º and 50.93º, consecutively. Chitosan affects an increase of the SPR signal toward the reflectivity where the SPR angle exists. These results imply a future prospective application of the Fe_3O_4/Chitosan as a signal amplifier material for the SPR sensor.**

Keywords—Fe_3O_4/chitosan, Surface Plasmon Resonance (SPR), signal amplifier

I. INTRODUCTION

The Fe_3O_4 nanoparticle has been attained a great deal of interest for researchers in the field of science and engineering. The nanoparticles have many potential applications due to their physical and chemical properties. The physical properties include mechanical, electrical, electronic structure, acoustic, optical, and magnetism (especially superparamagnetism). However, the chemical properties include surface structure, reactivity, solubility, dispersibility, surface energy, and oxidation process [1]. Especially, in the field of biomedical technology, the Fe_3O_4 has been applied as a cancer drug loader [2], hyperthermia heating agent [3], the treatment of central nervous system disorders, photoablation theraphy, photodynamic therapy, targeted drug delivery, theranostic application, and biosensor [2–6].

The Fe_3O_4 nanoparticle has been used widely as active material in many types of the sensor due to their active and high surface area to volume ratio [7], high electron exchange rate [8], excellent adsorption, and inherent electrical conductivity [9]. Those sensors are electrochemical sensors [7,9–11], magnetic sensors [11–14], and optical sensors, such as surface plasmon resonance (SPR) based sensor [15–17]. The SPR-based sensor is commonly regarded as Otto and Kretschmann configuration. Using the Kretschmann configuration, so the Fe_3O_4 nanoparticles are layered on the surface of a metallic thin film, for instant gold and silver (see Figure 1). Deposition of Fe_3O_4 layer onto film surface is proposed to improve the SPR biosensing performance. The Fe_3O_4 takes a role as a dielectric medium. This dielectric layer guides optical waves in transverse electric modes. The Fe_3O_4 layer can produce a much larger refractive index change at the evanescent field of the gold or silver surface-bound molecules during the biorecognition process [18]. Hence, the SPR is excessively sensitive to the change of that refractive index. The coupling between Fe_3O_4 and the secondary biomolecules linked with the gold or silver thin film leads to an increment of the refractive index change and more mass concentration on the sensor surface. Therefore, they will amplify the signal response

of the SPR sensor at the interface and affect sensitivity enhancement, such as performed by [15–17,19–21].

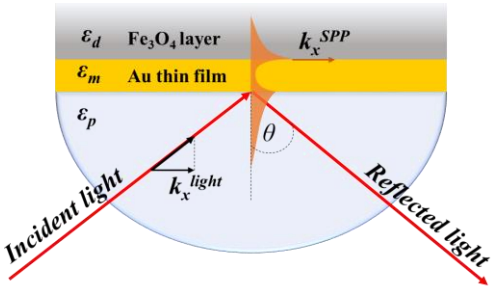

Fig. 1. Pictorial view of SPR-based sensor structure using Kretschmann configuration.

There are many issues with using Fe_3O_4 as a signal amplifier in the SPR-based sensor. First, these nanoparticles have low chemical stability and very sensitive to experience oxidation which can degrade their physical properties and performance. Second, the Fe_3O_4 nanoparticles may have a wide range of particle size distribution and non-uniform shape. This is a primary challenge for the synthesis of nanoscale particles because of the quantum confinement effect, so their properties strongly depend on the particle size. Third, due to their superparamagnetic properties in nature therefore the nanoparticles are easy to experience an irreversible agglomeration forming aggregates. Fourth, the Fe_3O_4 nanoparticles have the low surface ability for biological uses due to agglomeration and losing their magnetic properties in a biological environment [18]. Fifth, the bare Fe_3O_4 can't directly interact with any biological molecule due to no ligands appear on their surface. Sixth, the bare Fe_3O_4 nanoparticles have hydrophobic properties in nature so that they are really difficult to be dispersed in water [22].

Many efforts have been done by researchers to address those issues. First, applying an effective synthesis technique to prepare the nanoparticles, i.e., high energy ball milling [23], thermal decomposition, hydrothermal, microemulsion [4], pyrolysis [20], and chemical coprecipitation [2,15]. Second, controlling the synthesis parameter, such as synthesis temperature, pH, and calcination temperature [24,25]. Third, surface engineering of the nanoparticles via encapsulation by using polymers, i.e., synthetic polymers such as carboxy group modified amphiphilic polymers [21], polyvinyl alcohol (PVA), polyethylene glycol (PEG); natural polymers such as dextran, starch, gelatin, and chitosan [22]. Encapsulation of the surface nanoparticles by using polymer will enhance their surface reactivity to any biological molecule.

Among those polymers, chitosan is considered the best candidate for encapsulating the surface of Fe_3O_4 in case of their application to detect biological molecules, for instant urea and creatinine by using an SPR-based sensor. Chitosan is a hydrophilic, biocompatible, and organic polymer [22]. This polymer has excellent characteristics of high biodegradability and low toxicity [26]. The most important thing about chitosan is having high molecular weight. That is important in its application on the SPR-based sensor to amplify the SPR-signal response and sensitivity.

In this research, we focus to investigate the optical properties of Fe_3O_4/chitosan nanocomposites and their application in the SPR-sensor system. Studying the optical properties of the nanocomposites is a very promising step to provide optical parameters data of the nanocomposites that will be used for studying the SPR-phenomenon. Herewith, we calculate the optical parameters, such as absorbance (A), absorption coefficient (α), refractive index (n), extinction coefficient (k), optical gap energy (E_g), and Urbach energy (E_u).

II. Methods

A. Synthesis of Fe_3O_4/Chitosan Nanocomposite

Synthesis of Fe_3O_4 nanoparticles was carried out using the coprecipitation method (see Figure 2). In this research, we used iron sand from Wari Ino Beach Halmahera Utara as the source of Fe^{2+} and Fe^{3+} ions. First of all, the Fe solution was prepared by dissolving 25-gram iron sand within 30 ml HCl (12 M). The iron sand was stirred at a temperature of 70°C and stirring rate 500 rpm to dissolve Fe^{2+} and Fe^{3+} ions to be $FeCl_3$ and $FeCl_2$ solution. The Fe solution is transferred to the NaOH solution (5M) by using a droplet pipette while it was being stirred with constant stirring of 500 rpm and temperature of 80°C. The coprecipitation process took time for 60 minutes. The slurry was rinsed by using distilled water 5 times. After that, the slurry was heated in an oven at a temperature of 100°C for 4 hours.

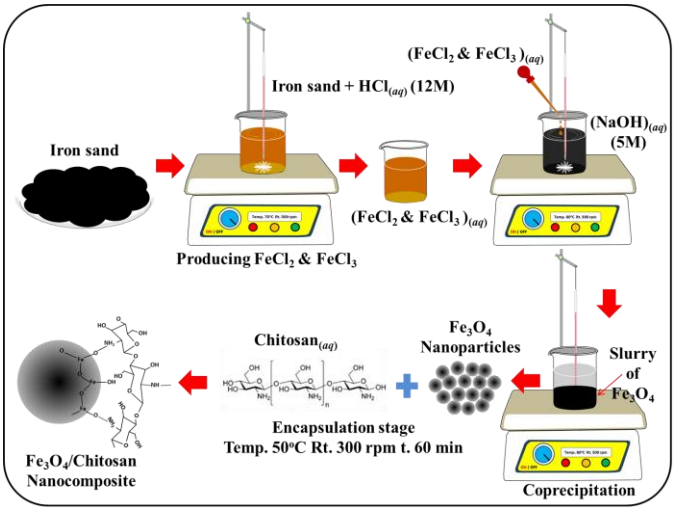

Fig. 2. Process of synthesizing Fe_3O_4/chitosan nanocomposites.

Powder Fe_3O_4 nanoparticles of 0.5 grams were dissolved with 50 ml distilled water in ultrasonic chamber for 30 minutes at room temperature. About 0.25 grams of chitosan powder were dissolved with 2wt% acetic acid to prepare the chitosan solution. This solution was dropped wisely to Fe_3O_4 solution

by using pipette while it was being stirred constantly of 300 rpm at a temperature of 50°C for 60 minutes. As result, the slurry of Fe_3O_4/chitosan nanocomposite was heated at a temperature of 60°C for 2 hours to provide powder nanocomposite.

B. Sample Characterizations

The samples were characterized using the X-ray diffraction (XRD) technique with a diffractometer instrument (PanAnalytical-Expert Pro) for their structural properties and phase composition. The diffraction data were recorded within an angle range of 20° – 80° (step size 0.02°) by using X-ray ($\lambda_{X\text{-}ray}$ = 1.540598 Å). However, the optical properties were characterized based on absorbance data gathered using UV-Vis Specular Reflectance Spectroscopy (Pharmaspec UV-1700).

C. SPR-Sensor Testing

Testing SPR-sensor mounted Fe_3O_4/chitosan was carried out by using the SPR instrument with a He-Ne laser beam (λ = 632.8 nm) within an incident angle range of 30° – 60°. BK7 prism (n ≈ 1.503) was used in this testing with gold lamination on its sensing surface via thermal evaporation. Kretschmann configuration was employed for this structure. The Fe_3O_4/chitosan solution was deposited onto the gold surface using the drop-casting method to form a dielectric layer.

III. Results and Discussion

A. X-ray Diffraction Pattern and the Structural Properties

The XRD patterns of Fe_3O_4 and Fe_3O_4/chitosan are depicted in Figure 3. The diffraction peaks are mostly well matched to the diffraction pattern of Fe_3O_4 according to JCPDS card no. 11-0467 and the result reported by [27]. There are seven peaks successfully identified in these patterns. The peaks are narrow and sharp, except for a peak of (533). Those imply that the samples are polycrystalline. The samples have high crystallinity. The long-range order of the crystallites is formed along their lattice direction. There is no other phase investigated within a sample of Fe_3O_4. On other hand, there is one extra phase investigated within a sample of Fe_3O_4/chitosan (*). This extra phase is γ-Fe_2O_3 (maghemite – JCPDS card no. 24-0081). However, the crystal structure of Fe_3O_4 and Fe_3O_4/chitosan is cubic spinel with a space group of *Fd3m*.

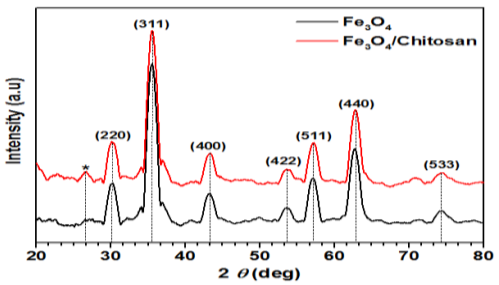

Fig. 3. XRD patterns of Fe_3O_4 and Fe_3O_4/chitosan.

The crystallite size of samples was calculated by using the Scherrer equation [28]. The crystallite size of Fe_3O_4 and Fe_3O_4/chitosan is 27.11 ± 0.04 nm and 27.97 ± 0.04 nm, consecutively. This indicates the chitosan layer onto the surface of Fe_3O_4 was successfully created. The lattice parameter of Fe_3O_4 and Fe_3O_4/chitosan is 8.401 ± 0.107 Å and 8.395 ± 0.108 Å, consecutively. These values mostly approach to standard lattice parameter of Fe_3O_4 provided in JCPDS card no.11-0467 (8.396 Å). The lattice parameter of Fe_3O_4/chitosan is shorter than Fe_3O_4 due to lattice contraction by encapsulation of the chitosan. This fact is consistent with the values of their lattice strain, i.e., 1.267 and 1.229. The lattice dislocation values are 1.360×10^{-3} nm^{-2} and 1.278×10^{-3} nm^{-2} for Fe_3O_4 and Fe_3O_4/chitosan.

B. Optical Properties

The optical properties include absorbance spectra (*A*), absorption coefficient (*α*), refractive index (*n*), extinction coefficient (*k*), optical gap energy (E_g), and Urbach energy (E_u). The absorbance spectra and absorption coefficient versus photon wavelength can be depicted in Figure 4. There are some absorption peaks successfully investigated on the spectra. Those peaks indicate different transitions occur to electrons when photon shined to the samples (photoexcitation). According to Figure 4a., the most number of the photon absorbed by electrons to do transition is in the wavelength of 333 nm and 329 nm, consecutively for Fe_3O_4 and Fe_3O_4/chitosan. This fact is supported by data of the absorption coefficient (Figure 4b). The absorption ability of Fe_3O_4/chitosan is higher than Fe_3O_4. This implies that more free electrons exist on the surface of Fe_3O_4/chitosan to do band-to-band transition by absorbing more photon. Physically, we can justify that Fe_3O_4/chitosan has a larger free electron concentration or larger Fermi level than bare Fe_3O_4. The largest value of photon energy absorbed by free electrons in Fe_3O_4 nanoparticles is about 4.38 eV (λ_{photon} = 283 nm). Hence, photon energy of 3.77 eV (λ_{photon} = 329 nm) is absorbed by electrons of Fe_3O_4/chitosan to do the highest interband transition.

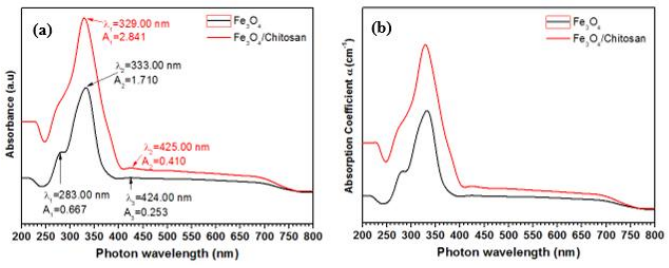

Fig. 4. (a) Absorbance spectra and (b) absorption coefficient of samples.

Figure 5 shows refractive index of samples for both real and imaginary values. The imaginary refractive index is represented by extinction coefficient (Figure 5b). Both Fe_3O_4 and Fe_3O_4/chitosan have real refractive index in a range of 1.50 – 2.75. These results are in a reasonable agreement to the research reported by [29]. The real refractive index of

Fe_3O_4/chitosan is higher then Fe_3O_4 for wavelength in the range of 450 nm - 750 (Figure 5a). At wavelength of 632.8 nm, real refractive index of Fe_3O_4 and Fe_3O_4/chitosan are 2.38 and 2.60, consecutively. In case of spectroscopy, the Fe_3O_4 nanoparticles have lower ability to absorb photon compared than Fe_3O_4/chitosan. This fact is physically supported by their values on the extinction coefficient and the absorption coefficient.

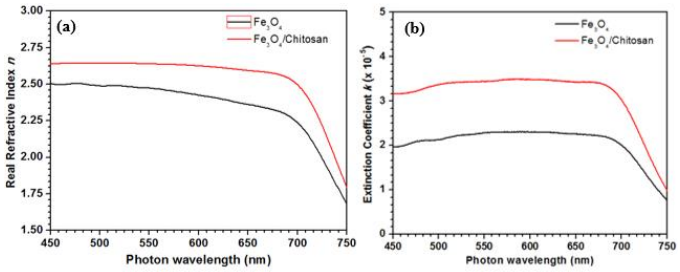

Fig. 5. (a) Real refractive index and (b) extinction coefficient of samples.

The interband transition of free electrons depends on the optical gap energy of the materials. There are two types of optical gap energy, i.e., direct and indirect optical gap energy [24]. Direct optical gap energy is the minimum energy needed by free electrons to directly across from the highest state of the valence band to the lowest state of the conduction band with the same vector momentum. On other hand, indirect optical gap energy is the total energy needed by free electrons to cross between those bands with different vector momentum. Hence, in this process, an electron is not only to absorb photon energy but also phonon energy. Pictorially, an illustration of the direct and indirect optical gap energy is depicted in Figure 6.

The estimation of the optical gap energies was carried out by employing Tauch's plot method. Both direct and indirect optical gap energy of Fe_3O_4 nanoparticles is greater than Fe_3O_4/chitosan. It is due to the quantum confinement effect. Larger particles size of nanoparticles will have smaller optical gap energy. This is consistent with the results of the absorbance spectra and the absorption coefficient. The optical gap values attained here are in agreement with the earlier results reported by [15,24].

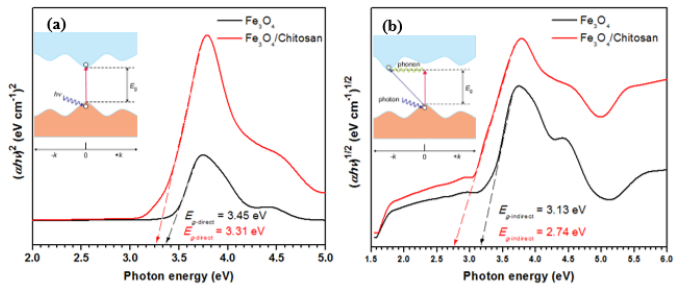

Fig. 6. (a) Direct and (b) indirect gap energy of samples [30].

Lattice strain and dislocation are examples of structural disorder of crystalline materials cause lattice imperfection. Lattice imperfection of Fe_3O_4 and Fe_3O_4/chitosan is not only directly influence their structural properties but also the electronic structure. At the atomic level, it influences the position of atoms. Lattice imperfection determines the occurrence of the bandtailing phenomenon. Bandtailing is the formation of band edges between the valence band (VB) and conduction band (CB) due to atomic disordering in the materials. These band edges are well known as the tail of density-of-states of electrons below the conduction band (E_{ct}) and above the valence band (E_{vt}) (see Figure 7a). The energy width of these band edges is known as Urbach energy. The existence of the electronic transitions between these band edges is empirically proved by data of the absorption coefficient (Figure 4b), where the absorption coefficient of samples exponentially decreases toward increment of photon wavelength. In another word, the absorption coefficient exponentially increases toward increment of photon energy [31]. Furthermore, the Urbach energy of Fe_3O_4 and Fe_3O_4/chitosan is 2.89 eV and 2.28 eV (see Figure 7b). Larger Urbach energy might be caused by larger lattice strain and dislocation. These results are in agreement with the earlier results reported by [15,24].

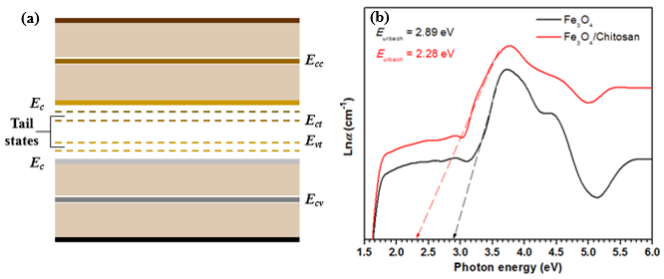

Fig. 7. (a) Ilustration of the band structure [32] and (b) Urbach energy of samples.

C. SPR-Sensor Testing

The SPR-sensor testing has been carried out by using a red laser with an excitation wavelength of 638.2 nm. The type of polarization mode was p-polarized. The SPR-sensor uses a Kretschmann configuration equipped with BK7 prims. The prism was deposited by gold with a dielectric constant of -9.39 ± 1.09i for the thickness of 50 nm [33]. On this configuration, we used three systems., e.g., prism/Au/air; prism/Au/Fe_3O_4/air; and prism/Au/Fe_3O_4-chitosan/air. Pictorially, the results can be depicted in Figure 8.

According to the SPR curves, a system of Prims/Au/Air produces the highest SPR signal. About 87.08% of the incident light was excited as surface plasmon polaritons (SPPs). Hence, systems of Prism/Au/Fe_3O_4/Air and Prism/Au/Fe_3O_4-chitosan/Air excite about 71.32% and 67.60% of the incident light as SPPs. Graphically, we can directly approximate that the FWHM of SPR curves for Prims/Au/Fe_3O_4/Air and Prism/Au/Fe_3O_4-chitosan/Air is much larger than the Prims/Au/Air system. The FWHM of the dip is associated with the attenuation of the surface plasmon. Distinct dips of the SPR curve are also associated with the transfer energy from an incident light wave into the surface plasmon resonance.

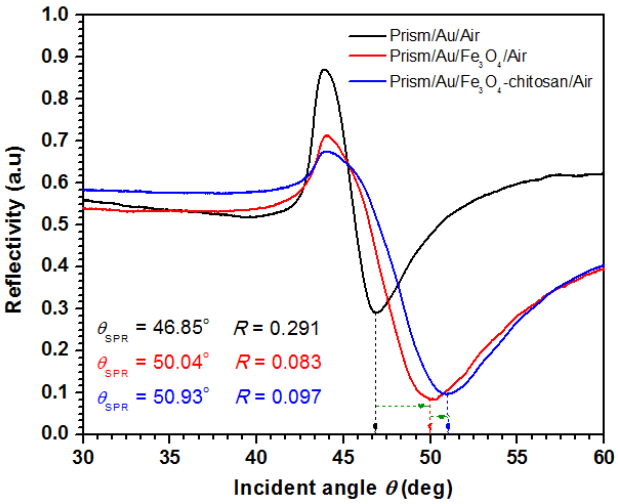

Fig. 8. SPR curves for Fe_3O_4 and Fe_3O_4/chitosan.

The SPR angle of the Prims/Au/Air system is 46.85°. This angle is shifted to 50.04° after the system is added by the Fe_3O_4 layer. The SPR angle is also shifted to a higher value (50.93°) after the system is added by Fe_3O_4/chitosan layer. These phenomena might be due to a change in the system's refractive index. The SPR angle of Prism/Au/Fe_3O_4-chitosan/Air is larger than Prims/Au/Fe_3O_4/Air due to refractive index change. The refractive index of Fe_3O_4/chitosan is larger than Fe_3O_4 (2.60 v.s 2.38 at a wavelength of 632.8 nm). According to these results, encapsulation of Fe_3O_4 with chitosan can amplify the SPR signal toward a change of the SPR angle shifted with a larger value. The results open chances for future work in the application of Fe_3O_4/chitosan nanocomposite for detecting targeted biomolecules.

IV. Conclusion

This research investigates the optical properties of Fe_3O_4/chitosan and its application for a signal amplifier in the SPR based sensor. The optical properties are affected by encapsulation. Encapsulation of Fe_3O_4 with chitosan polymer was proved able to increase the refractive index of the material and decrease the optical gap energy. Encapsulation makes nanocomposite having more free electrons on their surface therefore it improves the chemical reactivity of the surface. The major findings of this work confirm that Fe_3O_4/chitosan has a larger SPR angle than Fe_3O_4 due to a larger refractive index. In conclusion, the Fe_3O_4/chitosan can be applied for a signal amplifier in SPR based sensor.

Acknowledgments

Authors wishing to acknowledge the Government of Indonesia due to full financial support given by Kemenristek-Dikti toward PDP Research Grant year 2019-2020 with a contract number of 337/LL12/KM/2020. Great thanks would also deliver to LPPMP Universitas Halmahera for facilitating the administration of this grant. Special thanks would like to give to the Laboratory of Material Physics and Instrumentation, Department of Physics Universitas Gadjah Mada for the facilities and the laboratory services.

References

[1] S. P. Patil and V. V Burungale, "Physical and Chemical Properties of Nanomaterials," in Nanomedicines for Breast Cancer Theranostics, Elsevier Inc., 2020, pp. 17–31.

[2] A. Sirivat and N. Paradee, "Facile Synthesis of Gelatin-Coated Fe3O4 Nanoparticle: Effect of pH in Single-Step Co-precipitation for Cancer Drug Loading," Mater. Des., vol. 181, p. 107942, 2019, doi: 10.1016/j.matdes.2019.107942.

[3] M. E. Villamin and Y. Kitamoto, "Synthesis of Multifunctional Clustered Nano-Fe3O4 Chitosan Nanocomposite for Biomedical Applications," in AIP Conference Proceeding, 2018, vol. 020014, no. January, doi: 10.1063/1.5021927.

[4] S. Anwar, "Magnetic Iron Oxide Nanoparticles: Synthesis, Characterization and Functionalization for Biomedical Applications in the Central Nervous System," Materials (Basel)., vol. 12, no. 465, pp. 1–24, 2019.

[5] Y. P. Yew, "Green biosynthesis of Superparamagnetic Magnetite Fe3O4 Nanoparticles and Biomedical Applications in Targeted Anticancer Drug Delivery System : A Review," Arab. J. Chem., vol. 13, no. 1, pp. 2287–2308, 2020.

[6] A. V. V Nikezic, A. M. Bondzic, and V. M. Vasic, "Drug Delivery Systems Based on Nanoparticles and Related Nanostructures," Eur. J. Pharm. Sci., vol. 151, no. 105412, pp. 1–18, 2020.

[7] R. N. Suhanto, "Sonochemical Synthesis of Magnetic - Fe3O4/Graphene Nanocomposites for Label-Free Electrochemical Biosensors," J. Mater. Sci. Mater. Electron., pp. 1–13, 2020.

[8] H. Kumar, N. Kumari, and R. Sharma, "Nanocomposites (Conducting Polymer and Nanoparticles) Based Electrochemical Biosensor for the Detection of Environment Pollutant: Its Issues and Challenges," Environ. Impact Assess. Rev., vol. 85, no. 106438, pp. 1–14, 2020.

[9] N. T. A. Thu, H. V Duc, N. H. Phong, N. D. Cuong, N. T. V Hoan, and D. Q. Khieu, "Electrochemical Determination of Paracetamol Using Fe3O4/ Reduced Graphene-Oxide-Based Electrode," J. Nanomater., no. 7619419, pp. 1–15, 2018.

[10] Q. He, "Facile Electrochemical Sensor for Nanomolar Rutin Detection Based on Magnetite Nanoparticles and Reduced Graphene Oxide Decorated Electrode," Nanomaterials, vol. 9, no. 115, pp. 1–16, 2019.

[11] P. Tipsawat, U. Wongpratat, S. Phumying, N. Chanlek, K. Chokprasombat, and S. Maensiri, "Magnetite (Fe3O4) Nanoparticles : Synthesis , Characterization and Electrochemical Properties," Appl. Surf. Sci., vol. 446, pp. 287–292, 2018.

[12] S. A. Mitu et al., "Materials Fe3O4 Nanofluid Injected Photonic Crystal Fiber for Magnetic Field Sensing Applications," J. Magn. Magn. Mater., vol. 494, no. 165831, pp. 1–7, 2020.

[13] I. Nurpriyanti, I. Pardede, E. Suharyadi, T. Kato, and S. Iwata, "Detection of Fe3O4 Magnetic Nanoparticles using Giant Magnetoresistance (GMR) Sensor Based on Multilayer and Spin Valve Thin Films by Wheatstone Bridge Circuit," in IEEE, 2016, pp. 32–36.

[14] Y. Zhang, J. Xu, Q. Li, D. Cao, and S. Li, "The Effect of the Particle Size and Magnetic Moment of the Fe3O4 Superparamagnetic Beads on the Sensitivity of Biodetection," AIP Adv., vol. 9, no. 015215, pp. 1–6, 2019.

[15] I. P. T. Indrayana et al., "Synthesis, Characterization, and Application of Fe3O4 Nanoparticles as a Signal Amplifier Element in Surface Plasmon Resonance Biosensing," J. Online Phys., vol. 5, no. 2, pp. 65–74, 2020.

[16] N. Y. Ekariyani, D. P. Wardani, E. Suharyadi, B. S. Daryono, and K. Abraha, "The Use of Fe3O4 Magnetic Nanoparticles as the Active Layer

to Detect Plant's DNA with Surface Plasmon Resonance (SPR) Based Biosensor," in AIP Conference Proceeding, 2016, vol. 1755, pp. 1–6.

[17] M. Oktivina, D. T. Nurrohman, A. N. Q. Z. Rinto, E. Suharyadi, and K. Abraha, "Effect of Fe3O4 Magnetic Nanoparticle Concentration on the Signal of Surface Plasmon Resonance (SPR) Spectroscopy," in IOP Conf. Series: Materials Science and Engineering, 2017, pp. 1–8.

[18] F. Fathi, M. R. Rashidi, and Y. Omidi, "Ultra-sensitive Detection by Metal Nanoparticles-Mediated Enhanced SPR Biosensors," Talanta, 2018.

[19] Q. Li et al., "A Gold/Fe3O4 Nanocomposite for Use in a Surface Plasmon Resonance Immunosensor for Carbendazim," Microchim. Acta, pp. 186–313, 2019.

[20] J. Wang, Z. Zhu, A. Munir, and H. S. Zhou, "Fe3O4 Nanoparticles-Enhanced SPR Sensing for Ultrasensitive Sandwich Bio-Assay," Talanta, vol. 84, no. 3, pp. 783–788, 2011.

[21] J. Wang, A. Munir, Z. Zhu, and H. S. Zhou, "Resonance Sensing and Its Application for the Ultrasensitive Detection of Magnetic Nanoparticle-Enriched Small Molecules," Anal. Chem., vol. 82, no. 16, pp. 6782–6789, 2010.

[22] J. K. Xu, F. F. Zhang, J. J. Sun, J. Sheng, F. Wang, and M. Sun, "Bio and Nanomaterials Based on Fe3O4," Molecules, vol. 19, pp. 21506–21528, 2014.

[23] J. F. D. Carvalho, S. N. D. Medeiros, M. A. Morales, A. L. Dantas, and A. S. Carrico, "Synthesis of Magnetite Nanoparticles by High Energy Ball Milling," Appl. Surf. Sci., vol. 275, pp. 84–87, 2013.

[24] I. P. T. Indrayana, S. Tunang, Y. M. Huragana, N. M. Istiqomah, and E. Suharyadi, "A Comprehensive Study on the Microstructure and Optical Properties of Fe3O4 Nanoparticles by Variation of Temperature and NaOH Concentration," J. Online Phys., vol. 5, no. 1, pp. 6–17, 2019.

[25] I. P. T. Indrayana, L. A. Tjuana, M. T. Tuny, and Kurnia, "Nanostructure and Optical Properties of Fe3O4: Effect of Calcination Temperature and Dwelling Time," in Journal of Physics Conference Series, 2019, pp. 1–10.

[26] D. Q. Hoang et al., "Functionalization of Fe3O4 Nanoparticles with Biodegradable Chitosan-Grafted-mPEG for Paclitaxel Delivery," De Gryuter, vol. 5, pp. 459–466, 2016.

[27] F. Malega, E. Suharyadi, and I. P. T. Indrayana, "Synthesis and Characterization of the Microstructure and Functional Group Bond of Fe3O4 Nanoparticles From Natural Iron Sand," J. Ilm. Pendidik. Fis. Al-Biruni, vol. 07, no. 1, pp. 13–22, 2018.

[28] K. Petcharoen and A. Sirivat, "Synthesis and Characterization of Magnetite Nanoparticles via the Chemical Co-precipitation Method," Mater. Sci. Eng. B, vol. 177, no. 5, pp. 421–427, 2012.

[29] E. Y. Levitin, N. G. Kokodiy, V. A. Timanjuk, I. O. Vedernikova, and T. M. Chan, "Measurements of the Size and Refractive Index of Fe3O4 Nanoparticles," Inorg. Mater., vol. 50, no. 8, pp. 881–884, 2014.

[30] R. J. D. Tilley, Colour and the Optical Properties of Materials: An Exploration of the Relationship Between Light, the Optical Properties of Materials and Colour. United Kingdom: John Wiley & Sons, Ltd., 2011.

[31] I. Studenyak, M. Kranjcec, and M. Kurik, "Urbach Rule in Solid State Physics," Int. J. Opt. Appl., vol. 4, no. 3, pp. 76–83, 2014.

[32] S. Kasap, C. Koughia, S. K. O'Leary, H. Ruda, and J. Singh, "Optical Properties of Electronic Materials: Fundamentals and Characterization," in Springer Handbook of Photonic and Electronic Materials, S. Kasap and P. Capper, Eds. New York: Springer Science+Business Media, Inc., 2006, pp. 57–63.

[33] W. M. Mukhtar, R. M. Halim, K. A. Dasuki, A. R. A. Rashid, and N. A. M. Taib, "SPR Sensor for Detection of Heavy Metal Ions : Manipulating the EM Waves Polarization Modes," Malaysian J. Fundam. Appl. Sci., vol. 13, no. 4, pp. 619–622, 2017.